Preparation of fouling resistant and highly perm-selective novel PSf/GO-vanillin nanofiltration membrane for efficient water purification

Sudesh Yadav[1], Ibrar Ibrar[1], Akshaya K. Samal[2], Ali Altaee[1, #], Sébastien Déon[3], John Zhou[1], Noreddine Ghaffour[4]

1: Centre for Green Technology, School of Civil and Environmental Engineering, University of Technology Sydney, 15 Broadway, NSW, 2007, Australia

2: Centre for Nano and Material Sciences, Jain University, Jain Global Campus, Ramanagara, Bangalore - 562112, India

3: Institut UTINAM (UMR CNRS 6213), Université de Bourgogne-Franche-Comté, 16 Route de Gray, 25030 Besançon Cedex, France

4 : King Abdullah University of Science and Technology (KAUST), Water Desalination and Reuse Center (WDRC), Biological and Environmental Science and Engineering (BESE), 23955-6900 Thuwal, Saudi Arabia

Corresponding author email address: ali.altaee@uts.edu.au

Graphical abstract
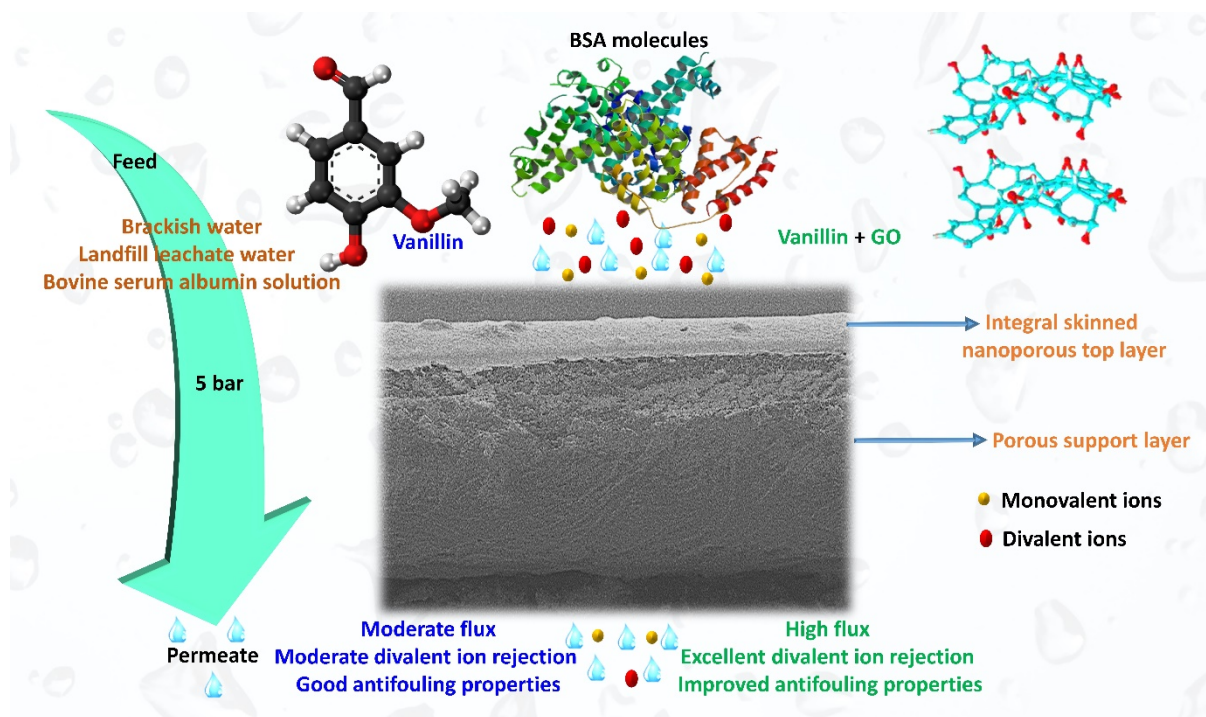
Abstract

To meet the rising global demand for water, it is necessary to develop membranes capable of efficiently purifying contaminated water sources. Herein, we report a series of novel polysulfone (PSf)/GO-vanillin nanofiltration membranes highly permeable, selective, and fouling resistant. The membranes are composed of two-dimensional (2D) graphite oxide (GO) layers embedded with vanillin as porogen and PSf as the base polymer. There is a growing interest in addressing the synergistic effect of GO and vanillin on improving the permeability and antifouling characteristics of membranes. Various spectroscopic and microscopic techniques were used to perform detailed physicochemical and morphological analyses. The optimized $PSf_{16}/GO_{0.15}$-vanillin$_{0.8}$ membrane demonstrated 92.5% and 25.4% rejection rate for 2000 ppm magnesium sulphate ($MgSO_4$) and sodium chloride ($NaCl$) solutions respectively. Antifouling results showed over 99% rejection for BSA and 93.57% flux recovery ratio (FRR). Experimental work evaluated the antifouling characteristics of prepared membranes to treat landfill leachate wastewater. The results showed 84-90% rejection for magnesium (Mg^{+2}) and calcium (Ca^{+2}) with 90.32 FRR. The study experimentally demonstrated that adding GO and vanillin to the polymeric matrix significantly improves fouling resistance and membrane performance. Future research will focus on molecular sieving for industrial separations and other niche applications using mixed matrix membranes.

 Keywords: PSf/GO-vanillin membrane; mixed matrix membrane; nanofiltration; fouling resistant; and salt rejection

1. Introduction

Water scarcity and pollution require advanced water purification technologies to produce potable water from non-common wastewater sources [1, 2]. Hazardous wastewaters, such as industrial and landfill leachate wastewaters, pose a threat to the ecosystem when discharged without proper treatment due to the high concentration of dissolved ions, heavy metals, pesticides and organic matters [3]. Despite the strict environmental regulations, deliberate and accidental waste release are on the rise [3, 4]. Conventional primary and secondary treatments have shown limited efficiency towards emerging pollutants. Tertiary treatments such as adsorption, photocatalysis, and membrane-based processes have been proven successful [5]. While membrane processes have the advantage over traditional treatment

49 technologies, they currently experience setbacks represented by fouling and membrane
50 permselectivity [5, 6].

51 At present, polyamide-based thin-film composite (TFC) membranes occupy the highest
52 portion in reverse osmosis (RO) and nanofiltration (NF) membranes technology for
53 desalination and wastewater treatment [7]. Still, TFC membranes have some shortcomings,
54 including low permeability, hydrophobicity, and fouling tendency [8]. NF membranes
55 effectively remove hazardous heavy metal ions and organic substances from solutions [9, 10],
56 but they are prone to fouling and exhibit low rejection of monovalent salts [11]. Thus, efforts
57 are made in fabricating novel NF membranes to overcome fouling by introducing diverse
58 nano-fillers, such as silver (Ag) [12], titanium oxide (TiO_2) [13], metal-organic frameworks
59 (MOFs) [14], graphene quantum dots [15], molybdenum disulfide (MoS_2) [16], and other
60 organic additives [17]. Although previous research has demonstrated the effectiveness of
61 these materials to tune the free volume characteristics of polymers, boundary defects
62 between polymers and nanomaterials are a challenging problem [18]. Further, many studies
63 have failed in providing information on the interfacial compatibility and gradual detachment
64 of nanomaterials over extended periods [19].

65 The development of specific molecular separation membranes is gaining considerable
66 attention. As a result, new research studies are focused on the fabrication of membranes with
67 specific molecular weight cut-offs by altering the surface characteristics, pore size
68 distribution, and changing solute diffusion parameters. In general, artificial grafting, surface
69 modification, chemical cross-linking, and in-situ physical blending are suggested for
70 enhancing membrane surface properties such as wettability, membrane fouling, pore
71 diameter, and surface zeta potential [20, 21]. Among the techniques mentioned above,
72 physical blending is the most effective strategy due to its suitability for large-scale production.
73 For instance, Yuan et al. prepared polyaniline (PANI)/polysulfone (PSf) membrane with better
74 water permeability and resistance to fouling [22]. For bovine serum albumin (BSA), humic acid
75 (HA), and sodium alginate (SA), the flux recovery ratio (FRR) was up to 65.3 %, 67.9 %, and
76 70.1 %, respectively [22]. In another study, PANI-graphene oxide nanofillers were used to
77 prepare polyvinylidene fluoride (PVDF) composite membrane for removing Allura red (AR)
78 and methyl orange (MO) dye from textile effluents [23]. PANI-GO nanofillers reduced the
79 water contact angle (WCA) to 56.11° and increased the pure water flux (PWF) from 112 to 454

80 LMH. With 95 % rejection of MO dye and 98 % of AR dye, the FRR reached 94 % [23]. Recently

81 Shu et al. used micron-sized 2-dimensional MOF (BUT-203) nanosheets to prepare mixed

82 matrix membrane for dye desalination rejection [24]. The findings suggested that chemical

83 cross-linking between polymers and nanofillers improves the membrane performance,

84 whereas dense separation layer and filler-loading limits the membrane performance [23, 24].

85 Pandey et al. developed fouling resistant MXene ($Ti_3C_2T_X$)/cellulose acetate (CA) covalently

86 cross-linked membrane, which showed PWF of 256.85 L m^{-2} h^{-1} bar^{-1} and over 92% rejection

87 for rhodamine B (RhB) dye [25]. The 10% @$Ti_3C_2T_X$/CA membrane demonstrated outstanding

88 antibacterial properties against E. coli and B. subtilis bacteria [25]. They achieved an ideal

89 separation by optimizing the filler-loading and adjusting the membrane pore size. However,

90 current NF membranes have poor antifouling properties and low water flux, which increases

91 energy consumption, making them unsuitable for treating complex wastewaters such as

92 landfill leachate. Thus, it is important to develop novel antifouling and high perm-selective NF

93 membranes for water and wastewater treatment.

94 Graphite oxide (GO) is a promising material widely used in membrane fabrication as a

95 nanofiller to improve water flux and reduce membrane biofouling due to its chlorine

96 tolerance and antimicrobial properties [26]. For instance, Ganesh et al. developed a mixed

97 matrix membrane with GO for salt rejection [27]. At 4 bar pressure, the prepared 2000 ppm

98 GO/PSf membrane showed near 48 LMH water flux and 74 % sodium sulfate (Na_2SO_4)

99 rejection [27]. Wu et al. prepared hybrid silica nanoparticles (SiO_2)-GO/PSf membranes and

100 achieved 98% rejection for egg albumin [28]. The prepared membranes showed 72% FRR with

101 enhanced antifouling properties [28]. In our previous work, an antifouling PSf/vanillin

102 composite membrane was prepared and achieved 99% rejection for BSA with 88.55% FRR

103 [17]. Vanillin imparts a negative surface charge and hydrophilic properties to the membrane

104 due to high polar surface area (46.53 $Å^2$) and functionalized phenolic ring [17, 29]. The current

105 work investigates the synergistic effect of 2D GO nanolayers and vanillin on membrane

106 permeability and selectivity using PSf as the base polymer. To the best of the authors'

107 knowledge, no study has reported GO-vanillin membrane performance for wastewater

108 treatment. The study presented an experimental work on a novel PSf/GO-vanillin membrane

109 for landfill wastewater treatment. The current study proposed cross-linked GO/vanillin to

110 enhance the wettability and fouling resistance of hydrophobic PSf membranes. The

111   antifouling and hydrophilicity properties of vanillin and GO will impart special features to the

112   fabricated membrane for landfill wastewater treatment. Antifouling studies were performed

113   using landfill leachate wastewater and BSA (200mg/L) solution. Magnesium sulphate ($MgSO_4$)

114   and sodium chloride (NaCl) were used as model salts for salt rejection studies.

115   **2.   Materials**

116   **2.1.   Chemicals**

117   In this study, all chemicals are of analytical grade and have not been further purified. N-

118   Methyl-2-pyrrolidone (NMP), PSf (≈ 35kDa), and BSA (Agarose Electrophoresis: > 98%;

119   Nitrogen: 14.5-16.5% and pH (1% in 0.15 M NaCl): 6.5-7.5) were obtained from Sigma-Aldrich

120   Australia. GO produced by Hummer's method (SKU: GTOP0003; brownish-yellow powder;

121   ~99% purity; 0.5-5 μm lateral size; 1-3 nm thickness; and ≤46.0 wt.% oxygen content) was

122   purchased from Advanced Chemicals Supplier (ACS) Material, LLC., CA 91106, USA.

123   Hydrochloric acid (HCl) was purchased from Merck. Sodium hydroxide (NaOH), NaCl, and

124    $MgSO_4$ used in the rejection test were procured from Chem-supply, Australia. Throughout the

125   experiments, deionized (DI) water (Milli-Q®, Merck) was used in the membrane fabrication

126   process. DI water was used to prepare the standard NaCl, $MgSO_4$, HCl, NaOH, and BSA

127   aqueous solutions for filtration tests. Biologically treated landfill leachate wastewater was

128   collected from Hurstville Golf Course, NSW, Australia (**Table 1**).

129   **Table 1**: Characteristics of landfill leachate wastewater used for this study.

| Characteristic	Value
Appearance	Dark Yellowish-brown colour
pH[a]	7.5 ± 0.3
Ammonia, mg/L	≤ 0.5
Total suspended solids, mg/L	27-117
Total dissolved solids (TDS)[a], mg/L	3300
Total organic carbon (TOC)[b], mg/L	120.5 ± 3.6
Total Iron, mg/L	3.5-5.2
Sodium (Na)[c], mg/L	142.05
Magnesium (Mg)[c], mg/L	125.3
Potassium (K)[c], mg/L	39.5

Calcium (Ca)[c], mg/L	65.4

130 [a]: measured using LAQUA PC210 conductivity metre; [b]: measured using analytikjena TOC;

131 and [c]: measured using Agilent Technologies 7900 ICP-MS.

2.2. Membrane fabrication

133 Non-solvent induced phase separation technique was applied for fabricating PSf-GO/vanillin

134 composite membranes, using N-Methyl-2-pyrrolidone (NMP) solvent, PSf base polymer, DI

135 water non-solvent, and vanillin as a pore-forming agent. Initially, a measured amount of GO

136 was exfoliated in NMP using Powersonic, Digital Ultrasonic Bath for an hour. The optimized

137 vanillin concentration, 0.8 g, was dissolved in GO-NMP dispersion for an hour using a

138 magnetic stirrer [17]. Then, PSf was gradually added to the GO-vanillin-NMP solution at 60 °C.

139 To obtain a homogeneous casting solution, the casting solution was stirred for 24 hours, and

140 an ultrasonication bath was used to release the trapped air bubbles. A glass plate was used

141 to case the prepared solution, using a stainless steel casting knife of 200 μm thickness before

142 transferring to a DI water coagulation bath (**Figure 1**). Finally, the PSf/GO-vanillin composite

143 membranes were transferred to a freshly prepared coagulation bath. The liquid-liquid

144 demixing for PSf-GO/vanillin membranes is shown in **Figure 2**. The membranes left there for

145 24 hours to ensure that the NMP solvent was completely removed. The chemical composition

146 of obtained membranes is tabulated in **Table 2**. The membrane fabrication process was

147 performed under ambient conditions of ~52% humidity and temperature at 22 °C.
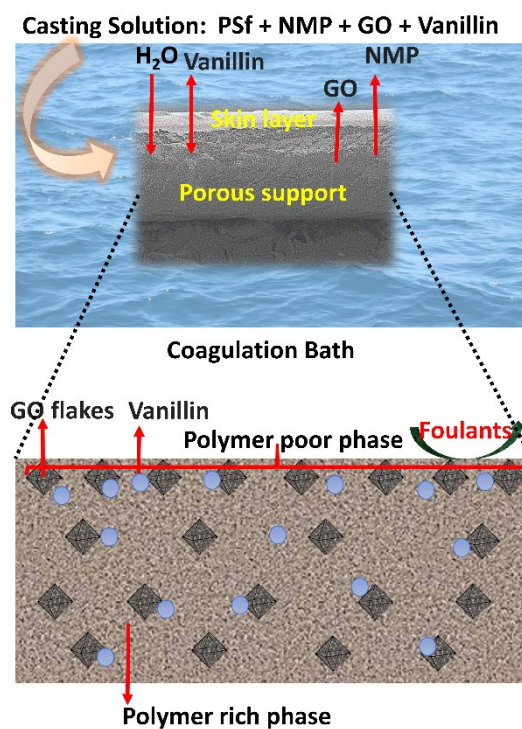

148
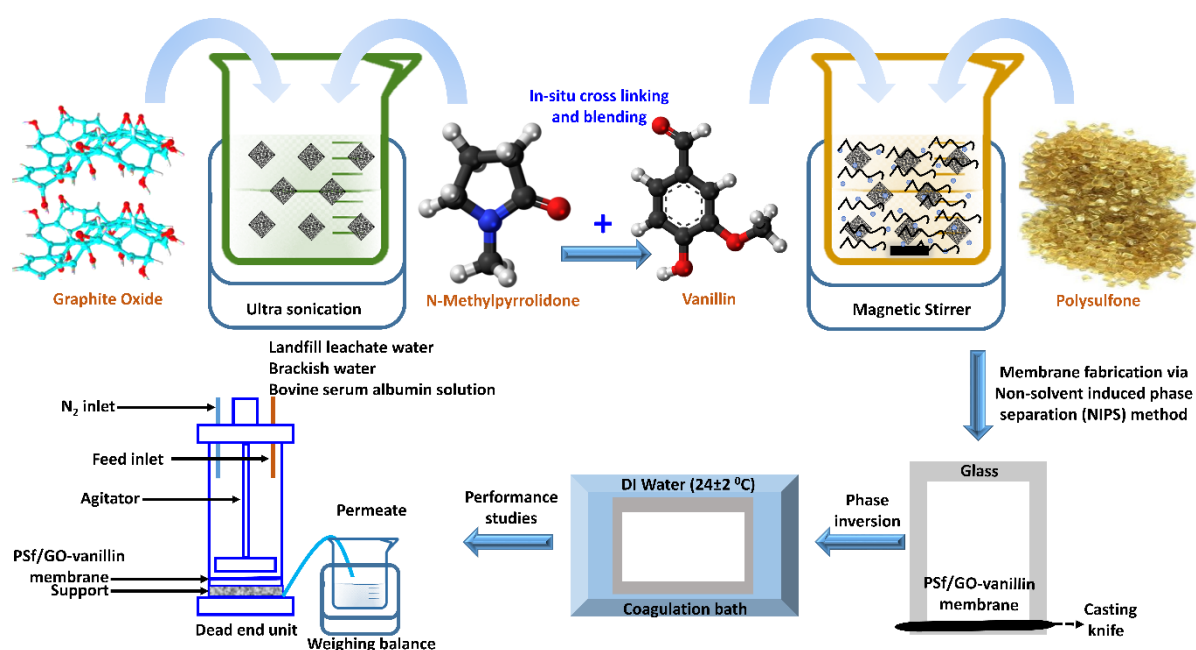
Figure 1: An illustration of the fabrication process for PSf-GO/vanillin composite membrane via in-situ cross-linking and blending.

Table 2: Chemical composition of casting solution used for fabrication of PSf-GO/vanillin composite membranes.

Membrane	PSf (g)	NMP (mL)	Vanillin (g)	Graphite oxide (mg)
M_1	3.2	16	0.8	0
M_2	3.2	16	0.8	50
M_3	3.2	16	0.8	100
M_4	3.2	16	0.8	150
M_5	3.2	16	0.8	200

Figure 2: Schematic illustration for the liquid-liquid demixing for PSf-GO/vanillin composite membrane.

2.3. Physiochemical characterization

The obtained membranes were characterised by various analytical tools mentioned in **Table 3**. Water uptake (WU) capacity was determined using previously dried membrane strips of 2

160 × 2 cm² surface area. After recording dried membrane weight (W$_d$), membrane strips were

161 then immersed 24 hours in DI water at 22 ± 2 °C. After carefully removing excess surface water

162 with absorbent paper, wet membranes were weighed (W$_w$). Finally, WU was determined

163 using Equation 1.

164 $$WU = \frac{(W_w - W_d)}{W_d} \times 100 \qquad (1)$$

165 Ion exchange capacity (IEC) of PSf-GO/vanillin membranes was measured using the back

166 titration method. Previously dried and weighed membrane strips (2 × 2 cm²) were immersed

167 in 0.5 M HCl solution for 24 hours at 22 ± 2 °C. Then, the membrane strips were removed from

168 the HCl solution, and the residual HCl solution was titrated with 0.05 M NaOH solution. Finally,

169 IEC was measured using Equation 2, where C_1, C_2, and V_1, V_2 are the concentration and volume

170 of HCl and NaOH, respectively.

171 $$IEC = \frac{C_1 V_1 - C_2 V_2}{W_d} \qquad (2)$$

172 **Table 3:** Various analytical tools used to characterise PSf-GO/vanillin composite membranes.

Analytical tool	Characteristics studied
Surface zeta (ζ) potential	To measure the surface charge of the membrane at interfaces
Fourier transform infrared (FT-IR)	For functional group and chemical structure analysis
Water contact angle (WCA)	For determining the wettability of the membrane's surface
Field emission scanning electron microscopy (FESEM)	To observe the surface morphological structures and cross-sectional area at the nanoscale

173

2.4. Membrane porosity and pore radius

175 The overall membrane porosity ε, which takes account of the various layers (i.e. skin and support

176 layers), was calculated from the weights of wet and dry membranes using Equation 3 [30]:

177 $$\varepsilon = \frac{\frac{w_w - w_d}{\rho_w}}{\frac{w_w - w_d}{\rho_w} + \frac{w_d}{\rho_p}} \qquad (3)$$

178 The densities of water and polymer are denoted by ρ_w and ρ_p in (g/cm^3), respectively.

179 The overall membrane pore radius (r_m) was estimated from pure water flux and porosity values

180 with the Guerout-Elford-Ferry Equation 4 [31]:

181 $$r_m = \sqrt{\frac{(2.9 - 1.75\varepsilon)\, 8\, \eta\, L\, Q}{\varepsilon\, A\, \Delta P}} \qquad (4)$$

182 The skin layer means pore radius was assessed by fitting salt rejection curves $R_{salt} = f(J_v)$ with a

183 usual transport model based on the coupling between Steric and Donnan exclusion at the

184 pore/solution interfaces and the extended Nernst-Planck equation (Equation 5) for transport

185 description. The various model equations were already presented in the literature [32, 33], and

186 the original methodology to estimate pore size from salt rejection was also detailed in a previous

187 study [17]. Briefly, it consists of adjusting the mean pore radius to fit experimental rejection of

188 MgSO$_4$, knowing the hydraulic permeability of the membrane is estimated from water flux

189 (considering Darcy's law) and membrane charge density from the zeta potential (considering the

190 Gouy-Chapman theory) [34, 35].

2.5.   Pure water flux and salt rejection studies

192 Filtration experiments were performed using a Sterlitech Company (USA) HP4750 dead-end

193 filtration cell with a 0.00146 m^2 membrane surface area (A). The processing volume of the

194 filtration cell was 300 mL. To ensure a constant permeate state at 5 bar operating pressure,

195 prepared membranes were compacted for 60 mins prior to initial readings using DI water feed

196 solution. After compaction, pure water flux (J$_W$) was measured in litres per square meter per

197 hour (L/m2h) for two hours using Equation 5, where the volume of permeate (V) was

198 calculated in litres (L) and permeation time (t) in hours.

199 $$J_W = \frac{V}{A \times t} \qquad (5)$$

200 The salt rejection studies were performed using 2000 ppm $MgSO_4$ and NaCl solutions as feed

201 for two hours. Every 10 minutes, the permeate rate was calculated using Equation 5. Three

202 trials of each set of experiments were conducted, and the average value is reported. The

203 concentrations of feed (C_f) and permeate (C_P) were measured by a conductivity metre (LAQUA

204 PC210), and the rejection rate was calculated using Equation 6. To minimize concentration

205 polarisation, a magnetic stirrer was used to mix feed solutions during the operation. C_f and C_P

206 for BSA solution and landfill leachate wastewater were measured using UV-Visible

207 spectrophotometer and inductively coupled plasma-mass spectrometry (ICP-MS).

208 $$Rejection\,(\%) = \left(1 - \frac{C_P}{C_f}\right) \times 100 \tag{6}$$

209 **2.6.   Antifouling studies**

210 The antifouling properties of the PSf-GO/vanillin composite membranes were investigated

211 using above mentioned filtration cell. Antifouling studies were conducted using 200 mg/L of

212 BSA feed solution and landfill leachate wastewater as feed solutions. All experiments were

213 performed at a constant 5 bar pressure with 14.6 cm^2 active surface area. After measuring

214 the water flux (J_1) of DI water for two hours, the BSA solution was the feed solution to

215 measure the water flux (J_P) in the dead-end experiment. Then, the membranes were washed

216 with DI water, and water flux decline (J_2) was measured using a DI water feed solution. Similar

217 experiments were performed for landfill leachate wastewater. Reversible (R_r), irreversible

218 (R_{ir}), total fouling (R_t), and FRR were determined using Equations 7 to 10.

219 $$R_r\,(\%) = \left(\frac{J_2 - J_P}{J_1}\right) \times 100 \tag{7}$$

220 $$R_{ir}\,(\%) = \left(\frac{J_1 - J_2}{J_1}\right) \times 100 \tag{8}$$

221 $$R_t\,(\%) = \left(1 - \frac{J_P}{J_1}\right) \times 100 \tag{9}$$

222 $$FRR\,(\%) = \left(\frac{J_2}{J_1}\right) \times 100 \tag{10}$$

223 **3. Results**

224 **3.1.   Functional group analysis**

225   FT-IR analysis was performed to study the functional groups of the prepared membranes. The
226   spectrum shows the percentage of infrared radiation that passes through the sample versus
227   a wavelength function related to covalent bonding. **Figure 3a** shows the FT-IR spectra for the
228   pristine PSf, PSf-vanillin, and PSf/Go-vanillin membranes from $1000cm^{-1}$ to $4000cm^{-1}$. FT-IR
229   spectra of PSf-vanillin and PSf/Go-vanillin membranes confirmed the existence of polar
230   functional groups on the surface. In the FT-IR, each stretching and bending vibration occurs
231   with a characteristic frequency. The stretching vibration of the hydroxyl (-OH) group for
232   vanillin and GO, which is stronger for PSf/Go-vanillin membranes than PSf-vanillin
233   membranes, is represented by the broad absorption and high-frequency area from $3024cm^{-1}$
234   to $3695cm^{-1}$ [17, 36]. This peak is noticeably absent in PSf membranes, as the PSf polymer
235   lacks any carboxylic acid or hydroxyl groups [37]. Additionally, the increase in intensity from
236   $3024cm^{-1}$ to $3695cm^{-1}$ indicates a strong intermolecular hydrogen bond between GO and
237   vanillin. PSf-vanillin and PSf/GO-vanillin membranes showed a low transmittance C-H
238   stretching peak at $2968cm^{-1}$. Pristine GO has a peak around $1615cm^{-1}$ that corresponds to the
239   bending vibration of -OH groups, but the peak shifts to $1643cm^{-1}$ with GO-vanillin [38]. The
240   change in peak position could be due to intermolecular hydrogen bonding between vanillin
241   and GO, as shown in **Figure 3b-d**. **Figure 3b-d** shows the intermolecular hydrogen bonding
242   epoxy, carboxyl, and hydroxyl groups of GO and vanillin. The peaks at $1242cm^{-1}$ and $1643cm^{-1}$
243   represent C-O-C stretching and C=C skeletal vibration of the GO, respectively [39]. Compared
244   to pristine PSf membranes, the change in frequency of peaks for PSf-vanillin and PSf/Go-
245   vanillin membranes could be due to mixing and redistribution of energy states, yielding new
246   energy levels because of intermolecular hydrogen bonding between PSf, vanillin, and GO, as
247   shown in **Figure 3c**. All membranes showed peaks for base polymer i.e. PSf at $1103cm^{-1}$ (S=O
248   stretching), $1149cm^{-1}$ (O–S–O symmetric stretching), $1489cm^{-1}$, and $1581cm^{-1}$ for aromatic
249   ring stretching [4, 40, 41]. The noise from $1500cm^{-1}$ to $1700cm^{-1}$ might be because of strong
250   π-π bond interactions from the aromatic rings of vanillin, GO, and PSf [4, 19].
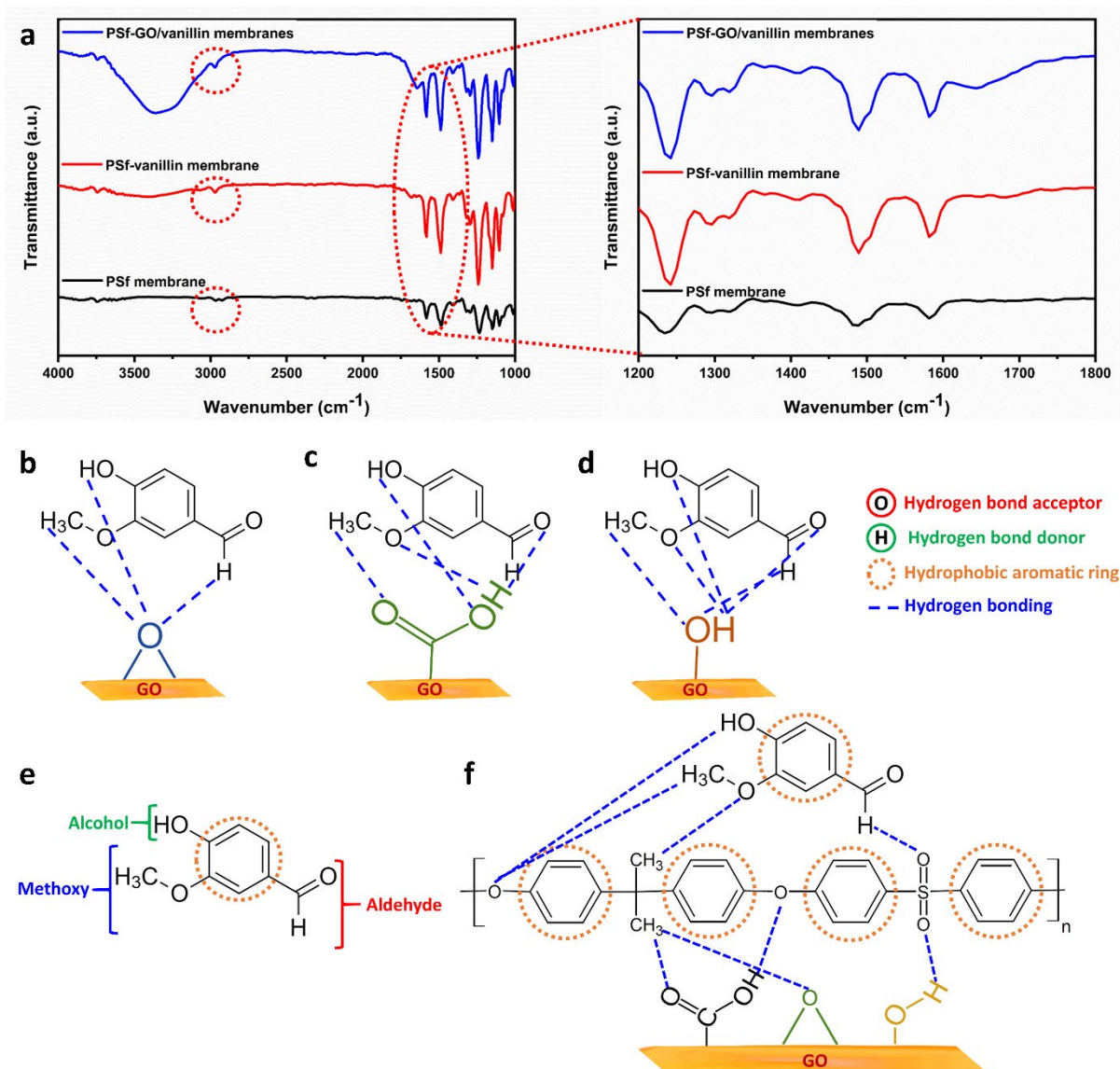
Figure 3: a) FT-IR spectra for PSf, PSf-vanillin, and PSf/GO-vanillin membranes, b-d) intermolecular hydrogen bonding between GO and vanillin molecules, e) functional groups and chemical structure of vanillin and f) intermolecular hydrogen bonding between PSf, GO, and vanillin molecules.

3.2.   Physiochemical characterization

It is worth noting that the membrane's IEC and WU are intricately related, and thus a systematic study of this relationship is necessary. The term "IEC" refers to the total polar functional groups on the membrane surface, and it measures their ionic conductivity [42]. **Figure 4a** shows the IEC and WU for PSf/GO-vanillin membranes. A larger IEC would increase

262 the membrane permeability and selectivity [43]. As expected, the incorporation of high polar

263 surface area vanillin (46.53 $Å^2$) and hydrophilic GO increases the WU and IEC capacity of the

264 prepared membranes [29]. With an increase in GO concentration, WU and IEC increases, and

265 the M_4 membrane showed the highest WU and IEC of 125.4% and 3.23 mmol/g, respectively.

266 When an excess GO was added to the casting solution, a decrease in WU and IEC was noticed

267 for the M_5 membrane, probably, due to the agglomeration of GO flakes in the M_5 membrane,

268 which prevents the polar functional groups from being accessible. The increase in WU and IEC

269 for PSf/GO-vanillin membranes is justified as following:

270 a) The addition of polar functional groups (carboxyl (-COOH), hydroxyl (-OH), aldehyde (-
271   CHO), and epoxy (-O-)) gives an additional negative charge to the membranes.

272 b) GO, and vanillin have the ability to bound water (H_2O) molecules via intermolecular
273   hydrogen bonding.

274 c) Vanillin imparts porosity to the membranes, which enhances the water absorption on the
275   membrane surface.

276 Indeed, an increase in IEC leads to an increase in WU, leading to a higher permeation rate.

277 The increase in permeation rate is due to the increase in the diffusion rate of protons and

278 hydroxide ions via the Grotthuss mechanism [44]. When polar functional groups exist on the

279 membrane surface, protons are transferred by hydrogen bonding from one water (H_2O)

280 molecule to the next [45]. Similarly, the high mobility of hydroxyl ions (OH^-) in H_2O is due to

281 the rapid transfer of H^+ from H_2O to OH^- along with a series of intramolecular hydrogen-

282 bonded H_2O molecules [4, 45, 46].

283 **Figure 4b** shows the WCA measurements for PSf/GO-vanillin membranes; an upsurge in

284 wetting tendency decreases the membrane WCA and surface tension. The WCA provides

285 important information about solid-liquid integration, membrane surface roughness, and

286 hydrophilicity. The hydrophilicity of the membranes increases with increasing the GO

287 concentration. The M_1 membrane exhibited the highest WCA of 61.4°, with adding more GO

288 to the casting solution, WCA decreases to 56.03°, 55.63°, 53.23° and 50.31° for M_2, M_3, M_4,

289 and M_5, respectively. It is worth noting that GO significantly reduces the WCA, as the pristine

290 PSf membrane exhibits a WCA of over 70° [17, 47]. Additionally, a lower WCA results in higher

291 surface energy and interfacial tension, creating a strong, attractive force that pulls the liquid

292 molecules down. As a result, low WCA results in a high permeation rate.

293 Electrostatic interactions between charged ions in the feed solution and the membrane's skin
294 layer are critical for understanding the rejection mechanism [48]. **Figure 4c** shows the surface
295 zeta potential measurements for PSf/GO-vanillin membranes. As a result of carboxylic (-
296 COOH), hydroxyl (-OH), and sulfonyl (-O=S=O-) groups from PSf, GO, and vanillin molecules,
297 the fabricated membranes had a negative zeta potential [17]. The surface zeta potential
298 increased with the increasing GO concentration from -20.52 mV to -25.07 mV for M_1 and M_4
299 membranes. However, due to the agglomeration of GO flakes, a slight decrease in surface
300 zeta potential was observed for the M_5 membrane (-24.12 mV). This increase in negative zeta
301 potential promotes salt rejection and inhibits foulant adsorption on the membrane surface
302 [48, 49].
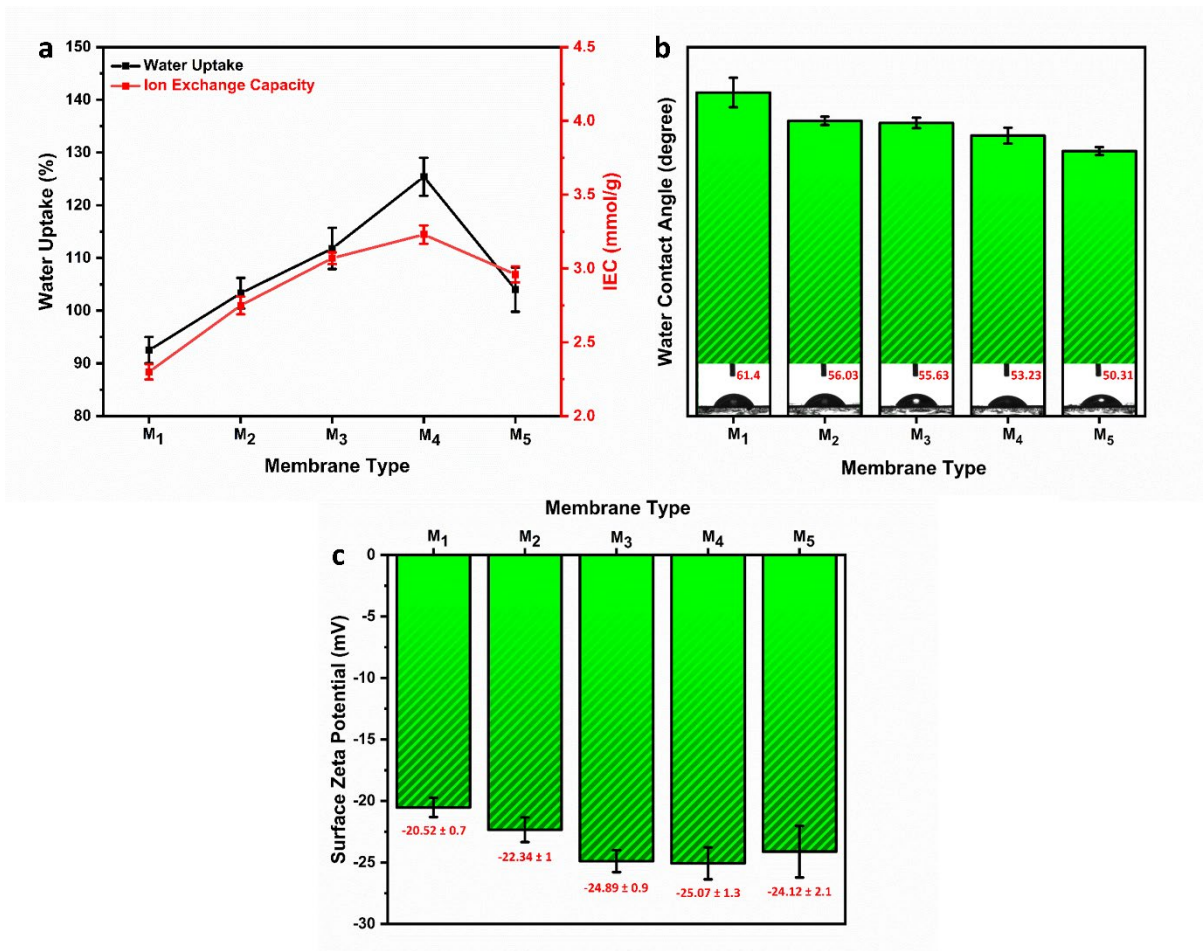
303

304 **Figure 4:** a) WU (water uptake) and IEC (ion exchange capacity) b) WCA (water contact angle),
305 c) surface zeta potential measurements for PSf/GO-vanillin membranes, and d) schematic
306 illustration for the membrane fabrication process.

307

308 ### 3.3. Porosity and mean pore radius

309 The membrane thickness L, the overall porosity ε, the overall membrane pore radius r_m and the

310 mean pore radius of the skin layer r_p obtained for the various membranes are summarized in

311 Table 4.

312 **Table 4**: Structural properties for PSf/GO-vanillin composite membranes.

Membrane	L (μm)	ε	r_m (nm)	r_p (nm)
M_1	97	0.54	7.05	0.55
M_2	108	0.56	7.71	0.54
M_3	113	0.59	7.9	0.54
M_4	121	0.61	8.36	0.53
M_5	101	0.56	10.85	0.84

313

314 As shown in **Table 4**, the thickness and overall porosity of the prepared membranes increases

315 as the GO content increases ($M_4 > M_3 > M_2 > M_1$), except for the highest GO content (M_5) for

316 which values are lower. This seems to show that it exists a limit GO amount above which both

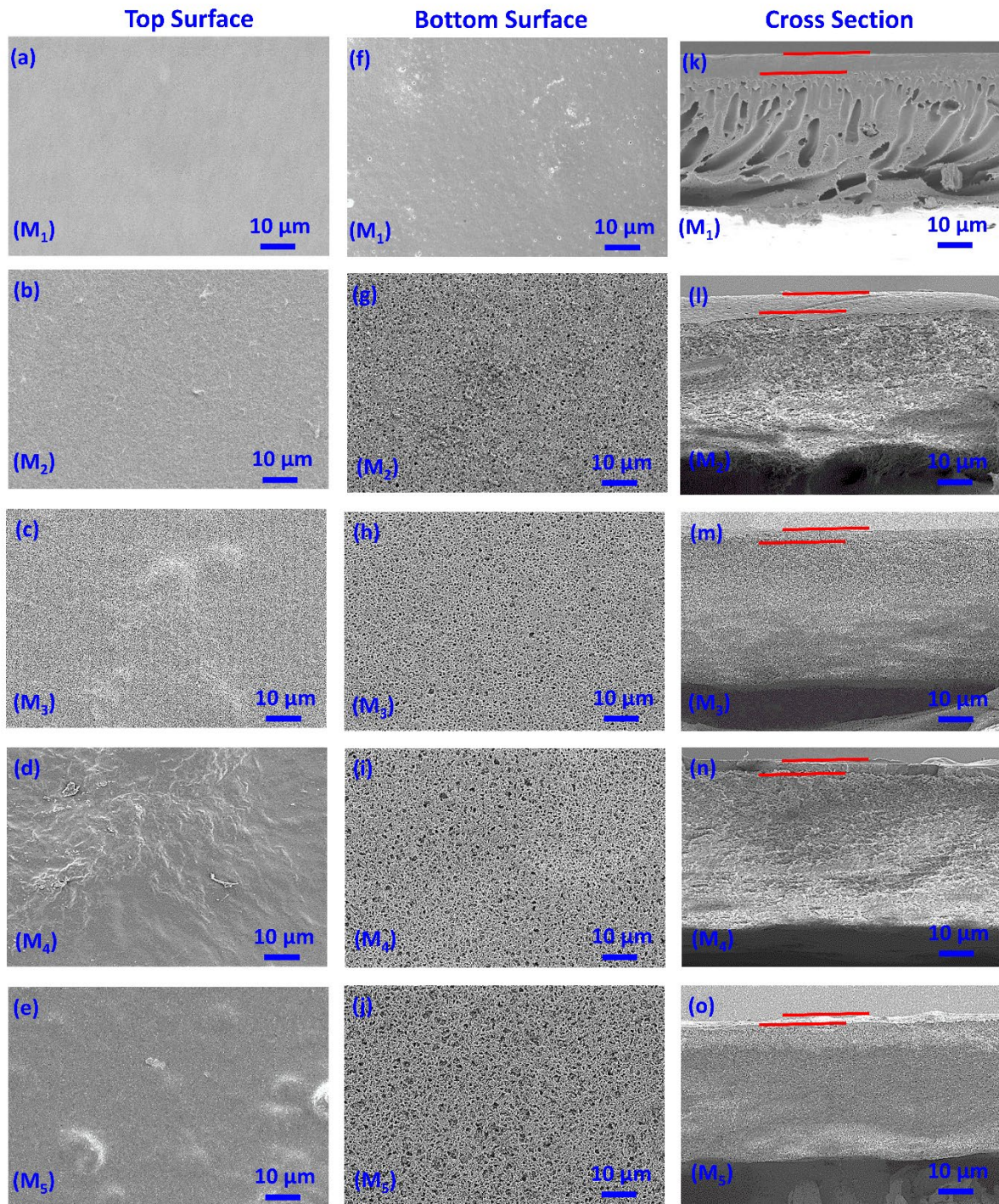317 thickness and porosity collapse.

318 The mean pore radius of membrane calculated by the Guerout-Elford-Ferry equation from

319 overall porosities shows the same trend, i.e. radius increases with GO content. However, it

320 should be emphasized that the mean pore radius of M_5 is markedly higher than that of M_1 to

321 M_4 membranes. The limit value observed with thickness and porosity does not have a

322 noticeable impact on the overall mean pore radius.

323 The skin layer properties were specifically studied from mean pore radii assessed by fitting

324 $MgSO_4$ rejection values. The obtained values are typical of NF membranes. It can be concluded

325 that the amount of GO does not have a considerable effect on the pore size of the skin layer

326 (0.54 ± 0.01 nm) up to 150 mg. Indeed, the M_5 membrane exhibits a strongly higher pore radius,

327 which means that the limit value of GO amount observable on overall membrane properties

328 (mainly support layers) also impacts the skin layer. This strong increases in skin layer pore size

329 is confirmed by the strongly higher permeability obtained with this membrane in the section

330 devoted to performances (Section 3.5).

331 **3.4.   Morphological analysis**

332 **Figure 5** shows the membrane morphology (top surface (a-e), a bottom surface (f-j), and

333 cross-section (k-o) for PSf/GO-vanillin membranes. The influence of GO and vanillin on

334 membrane morphology was investigated. Prepared membranes are integrally skinned

335 asymmetric with the dense top layer and microporous sublayer. The top-surface morphology

336 reveals that wrinkles are forming as GO loading increases. The wrinkled structure could be

337 caused by water molecules accumulating between the PSf polymeric chains and GO layers

338 (**Figure 5b-e**) [50]. These water molecules gradually drain and form wrinkles during the

339 membrane formation process. Instantaneous liquid-liquid demixing was observed for the M_1

340 membrane, whereas a slight delay in liquid-liquid demixing was observed after adding GO to

341 the casting solution (**Figure 2**). As a result, the M_1 membrane has finger-like cross-sectional

342 channels (**Figure 5k**), whereas M_2–M_5 membranes have a sponge-like structure, as evident by

343 FESEM analysis (**Figure 5l-0**). Additionally, the sponge-like structure could be a result of cross-

344 linking between GO and vanillin molecules. The solubility of vanillin in the solvent and non-

345 solvent used for membrane fabrication results in a porous network on the bottom surface of

346 the prepared membranes (**Figure 5f-j**).

Top Surface	Bottom Surface	Cross Section
(a) (M$_1$) 10 µm	(f) (M$_1$) 10 µm	(k) (M$_1$) 10 µm
(b) (M$_2$) 10 µm	(g) (M$_2$) 10 µm	(l) (M$_2$) 10 µm
(c) (M$_3$) 10 µm	(h) (M$_3$) 10 µm	(m) (M$_3$) 10 µm
(d) (M$_4$) 10 µm	(i) (M$_4$) 10 µm	(n) (M$_4$) 10 µm
(e) (M$_5$) 10 µm	(j) (M$_5$) 10 µm	(o) (M$_5$) 10 µm

Figure 5: Field emission scanning electron microscope (FESEM) images for PSf/GO-vanillin composite membranes.

3.5.   Performance studies

3.5.1. Pure water flux

353 The pure water flux (PWF) of PSf-vanillin and PSf/GO-vanillin composite membranes is shown

354 in **Figure 6a**. The addition of GO to the PSf-vanillin casting solution increases the membrane's

355 hydrophilicity, resulting in increased water molecule sorption on the membrane surface. The

356 WU and WCA studies showed a similar pattern. The addition of GO improved the porous

357 network and provided polar functional groups to the membrane surface, increasing PWF. A

358 PWF was also observed as the top layer thickness decreased from M_1 to M_5 membranes. The

359 PWF increased up to ≈ 91 LMH for the M_5 membrane. The PSf-vanillin (M_1) membrane had

360 the lowest PWF, ranging from 39-35 LMH. The slight decrease in PWF across all membranes

361 during operation could be due to membrane pore compression/collapse, resulting in reduced

362 water passage. Furthermore, the PWF could decrease due to the gradual loss of free volume.

363 **3.5.2. Salt rejection studies**

364 The 2000 ppm NaCl and $MgSO_4$ aqueous solutions were used as feed solutions for salt

365 rejection studies and passed perpendicularly through the membrane surface at constant 5

366 bar pressure. **Figures 6b and 6c** show water flux of PSf-vanillin and PSf/GO-vanillin

367 membranes using NaCl and $MgSO_4$. Experimental results showed that permeate flux

368 increased 2.5 fold from ≈ 35 to ≈ 88 LMH for the M_1 and M_5 membrane, respectively. The

369 decline in permeate flux during operation could be ascribed to surface/pore adsorption due

370 to electrostatic interaction between membrane and foulants. Also, permeate flux may be

371 reduced due to salt molecule accumulation on the membrane surface, increasing resistance.

372 However, continuous stirring was used to minimize concentration polarization effects

373 throughout the experiments. Additionally, increasing the water flux stimulates salt molecule

374 convection to the membrane, resulting in a decline in salt rejection of up to 61.04 ± 2.98 for

375 $MgSO_4$ and 10.14 ± 2.97 for NaCl for the M_5 membrane. The M_4 membrane showed the

376 highest rejection of 92.51 ± 2.73 and 25.43 ± 3.12 for $MgSO_4$ and NaCl, respectively. Compared

377 to the M_1 (PSf-vanillin) membrane, M_3 and M_4 (PSf/GO-vanillin) membranes showed a 4%

378 higher rejection for divalent ions, which could be due to the higher negative surface charge

379 of M_3 and M_4 membranes due to the presence of GO moieties (**Figure 6d**). In contrast, the

380 commercial UA 60 membrane showed the rejection rate of 77.13 ± 3.12 and 12.02 ± 2.94 for

381 $MgSO_4$ and NaCl, respectively [17]. All membranes showed better rejection for divalent ions

382 compared to the monovalent ions. The rejection results can be justified as following:

383 a) The PSf/GO-vanillin membrane charge and pore radius are vital in rejecting $MgSO_4$ and
384   NaCl solutions. Thus, the rejection mechanism in PSf/GO-vanillin membranes is governed
385   by both sieving and Donnan effects.
386 b) The sulphate (SO^{-2}) and chloride (Cl^-) ions are better repelled by the negatively charged
387   PSf/GO-vanillin membranes, and thus the bulk of these anions remains on the feed side.
388 c) As the SO^{-2} anion has a larger ionic radius (0.242 nm) than the Cl^- anion (0.181), the
389   prepared membranes showed better $MgSO_4$ rejection.
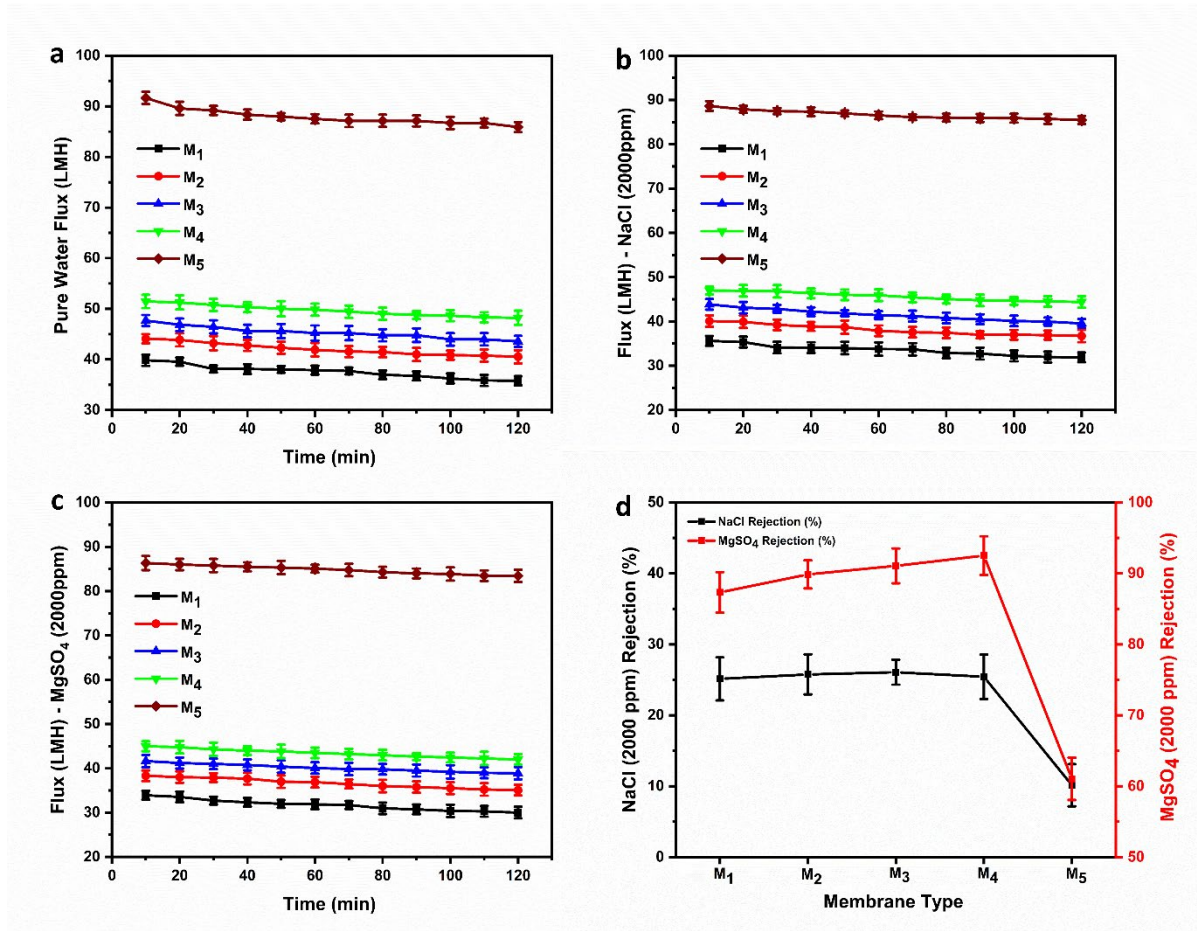
Figure 6: a) Pure water flux, b) and c) permeate flux of 2000 ppm sodium chloride (NaCl) and magnesium sulphate ($MgSO_4$) solutions respectively, and d) rejection rate of NaCl and $MgSO_4$ with PSf/GO-vanillin composite membranes.

3.6.   Antifouling studies

Membrane fouling by organic, inorganic and inert matters causes a sharp decline in the permeate flux. Technically, fouling is caused by physical and chemical interactions between the foulants and the membrane surface. As most foulants are non-polar or hydrophobic, preparing hydrophilic membranes is the most promising way to avoid fouling. Both vanillin

399 and GO are known for their hydrophilicity, anti-biofouling ability, and antibacterial properties

400 [17, 51]. Antifouling properties of PSf/GO-vanillin membranes were evaluated using BSA and

401 landfill leachate wastewater feed solutions. **Figure 7a** and **7d** show the permeation flux for

402 BSA and landfill leachate wastewater using PSf/GO-vanillin membranes. As expected, the

403 permeation rate decreased for all membranes when BSA and landfill leachate wastewater is

404 the feed solutions. Compared to the PSf-vanillin M_1 membrane, the water flux of M_2 to M_5

405 PSf/GO-vanillin membranes had better antifouling properties, manifested by higher water

406 flux recovery (**Figure 7**). For the BSA solution, the water flux decreased from 39.84 LMH to

407 23.87 LMH for M_1, 44.09 LMH to 31.76 LMH for M_2, 47.67 LMH, and 33.65 for M_3, 51.45 LMH

408 for M_4 and 91.64 LMH to 75.43 LMH for the M_5 membrane. When landfill leachate wastewater

409 was the feed solution, water flux dropped to 21.58, 29.85, 31.99, 34.56, and 72 LMH for M_1-

410 M_5 membranes, respectively. In both cases, the water flux decreased due to foulant

411 deposition on the membrane surface. Initially, foulants are deposited via convective

412 deposition; later, foulants are chemically attached to the foulant layer [17]. BSA molecules

413 form intermolecular disulphide linkages with the foulant layer [52]. Overall, the water flux

414 decline was higher in the experiments with landfill feed solution. The higher water flux decline

415 in landfill feed solution could be attributed to the interaction between organic and inorganic

416 matters that exacerbated the fouling mechanism. M_1 membrane showed the highest R_t

417 (39.2% and 50 %) for BSA and landfill leachate wastewater, respectively (**Figure 7b and e**). In

418 the M_5 membrane experiments using BSA and landfill leachate wastewater, the R_t decrease

419 was 14.9% and 19.98%, while the FRR was 93.57% and 90.32% (**Figure 7c and f**), respectively.

420 Obviously, casting solution contains GO enhanced the antifouling properties of the fabricated

421 membranes, and a higher water flux recovery was achieved for M_2-M_5 membranes. The M_1-

422 M_4 membranes had a rejection rate of over 99% for BSA; however, the M_5 membrane had a

423 lower rejection rate due to the porous network structure, as shown in **Figure 5j**. When landfill

424 leachate wastewater was the feed solution, the rejection rate for divalent ions (Mg^{+2} and Ca^{+2})

425 was higher than monovalent ions (Na^+ and K^+) (**Table 5**). Except for the M_5 membrane, all

426 other prepared membranes showed 84 to 90% rejection rate of Ca^{+2} and Mg^{+2} ions and 20 to

427 27% rejection rate of Na^+ and K^+ anions. A similar trend was observed for the salt rejection

428 studies (**Section 3.5.2.**). The $PSf_{16}/GO_{0.15}$-vanillin$_{0.8}$ membrane showed better antifouling and

429 salt rejection performance than the commercial UA60 nanofiltration membrane. The

430 antifouling properties of prepared membranes are justified as following:

431   a) The addition of GO increases the hydrophilicity of the membranes, resulting in a reduction

432   in the interaction between fouling matters and the membrane surface, thus reducing R_t,

433   R_r, and R_{ir}.

434   b) As R_t, R_r, and R_{ir} are inversely proportional to water flux recovery. The prepared

435   membranes demonstrated an increased FRR with increasing GO concentration.

436   c) These findings suggest that the negatively charged PSf/GO-vanillin membranes inhibited

437   the aggregation of negatively charged BSA and fouling matters on the surface.

438   Consequently, fouling matters could be easily removed by DI water washing.

439   Despite the higher permeation flux and antifouling properties of the M_5 membrane, the M_4

440   membrane demonstrated excellent rejection rates and water flux. M_4 membrane, therefore,

441   is the best performance membrane when used for landfill leachate wastewater treatment

442   compared to other membranes. For feed solution containing mainly divalent ions, the M_4

443   membrane could be an alternative to the M_1 membrane due to the superior water flux and

444   antifouling property. In other words, the M_4 membrane could have potential applications for

445   industrial wastewater treatment to remove heavy metals. These results indicated that

446   PSf/GO-vanillin membranes had improved antifouling properties compared to previously

447   reported PSf-vanillin membranes [17]. The use of vanillin results in an eco-friendly and cost-

448   effective additive for the membrane fabrication process. Asymmetric membranes using GO

449   and vanillin provide an easy, cost-effective and versatile approach for preparing highly

450   permeable and fouling resistant membranes.

451
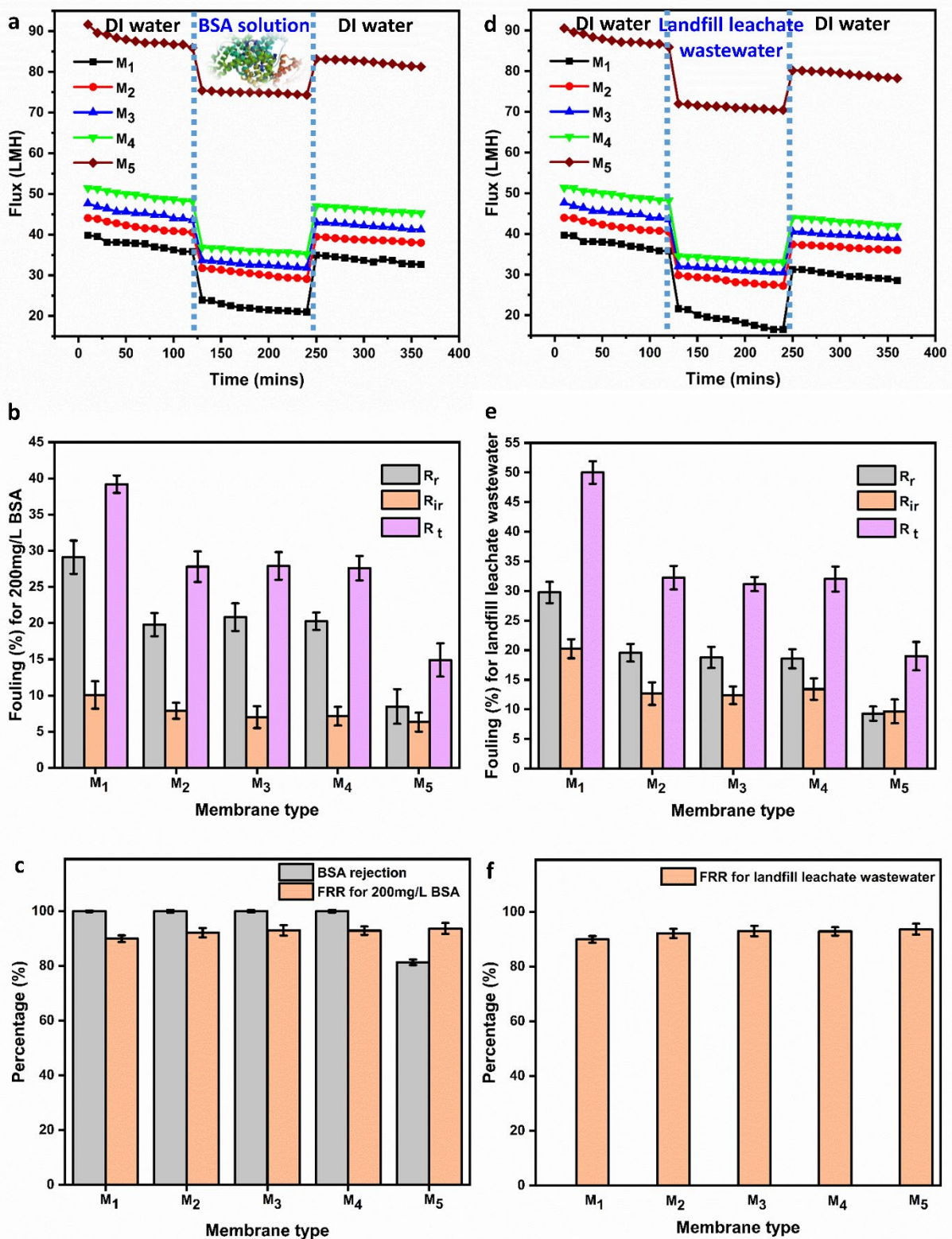
Figure 7: Flux measurements (a, d), fouling measurements (b, e) and flux recovery ratio (c, f)

for BSA and landfill leachate wastewater, respectively, with PSf/GO-vanillin composite

membranes.

Table 5: Concentration and rejection rate of different ions in landfill leachate wastewater with
456 PSf/GO-vanillin membranes.

Ion	Initial concentration (mg/L)	Rejection rate for M_1 (%)	Rejection rate for M_2 (%)	Rejection rate for M_3 (%)	Rejection rate for M_4 (%)	Rejection rate for M_5 (%)
Sodium (Na^+)	142.05 ± 5	21.12	22.42	23.56	23.52	8.2
Magnesium (Mg^{+2})	125.3 ± 5	84.87	88.21	89.75	90.12	60
Potassium (K^+)	39.5 ± 5	23.4	25.45	26.95	27.02	10.2
Calcium (Ca^{+2})	65.4 ± 5	85.24	88.85	89.25	90.2	62.45
Total organic carbon (TOC)	120.5 ± 3.6	85.3	88.8	90.2	92.7	68.7

457

4. Conclusions

A fouling resistant and highly perm-selective PSf/GO-vanillin nanofiltration membrane was fabricated for wastewater purification and recovery. The 2D GO layers and vanillin help to retain the structural integrity of the PSf based mixed matrix membranes. The present study concludes with the following key points:

a) The addition of 2D GO layers improves the membranes wetting, rejection, and antifouling properties.

b) Combining GO and vanillin enhances the negative surface zeta potential for the prepared membranes, and as a result, a higher rejection rate was observed for divalent ions.

c) The PSf/vanillin (M_1) membrane had a PWF of 39 LMH, but adding GO to the casting solution increased the PWF of the M_5 membrane to 91 LMH.

d) The optimized $PSf_{16}/GO_{0.15}$-vanillin$_{0.8}$ membrane showed 92.5% rejection for $MgSO_4$ solution, nearly 29% higher than the commercial UA 60 membrane, which rejects up to 77.13%.

e) The prepared membrane demonstrated a significantly higher FRR of 93.57% and 90.32% for BSA and landfill leachate wastewater, respectively.

474   f) The PSf/GO-vanillin membranes are potential candidates for robust and energy-efficient

475   water treatment because of their high flux and fouling resistance.

476

477   **References**

478   [1] P. Greve, T. Kahil, J. Mochizuki, T. Schinko, Y. Satoh, P. Burek, G. Fischer, S. Tramberend, R.
479   Burtscher, S. Langan, Global assessment of water challenges under uncertainty in water scarcity
480   projections, Nature Sustainability, 1 (2018) 486-494.
481   [2] S. Yadav, H. Saleem, I. Ibrar, O. Naji, A.A. Hawari, A.A. Alanezi, S.J. Zaidi, A. Altaee, J. Zhou, Recent
482   developments in forward osmosis membranes using carbon-based nanomaterials, Desalination, 482
483   (2020) 114375.
484   [3] I. Ibrar, S. Yadav, A. Altaee, A.K. Samal, J.L. Zhou, T.V. Nguyen, N. Ganbat, Treatment of biologically
485   treated landfill leachate with forward osmosis: Investigating membrane performance and cleaning
486   protocols, Sci. Total Environ., 744 (2020) 140901.
487   [4] S. Yadav, K. Soontarapa, M. Jyothi, M. Padaki, R.G. Balakrishna, J.-Y. Lai, Supplementing multi-
488   functional groups to polysulfone membranes using Azadirachta indica leaves powder for effective and
489   highly selective acid recovery, J. Hazard. Mater., 369 (2019) 1-8.
490   [5] P.S. Goh, T.W. Wong, J.W. Lim, A.F. Ismail, N. Hilal, Innovative and sustainable membrane
491   technology for wastewater treatment and desalination application, in: Innovation Strategies in
492   Environmental Science, Elsevier, 2020, pp. 291-319.
493   [6] S. Yadav, I. Ibrar, S. Bakly, D. Khanafer, A. Altaee, V. Padmanaban, A.K. Samal, A.H. Hawari, Organic
494   Fouling in Forward Osmosis: A Comprehensive Review, Water, 12 (2020) 1505.
495   [7] P. Bhol, S. Yadav, A. Altaee, M. Saxena, P.K. Misra, A.K. Samal, Graphene-Based Membranes for
496   Water and Wastewater Treatment: A Review, ACS Applied Nano Materials, (2021).
497   [8] S. Castelletto, A. Boretti, Advantages, limitations, and future suggestions in studying graphene-
498   based desalination membranes, RSC Advances, 11 (2021) 7981-8002.
499   [9] M. Mulder, Basic principles of membrane technology, Springer Science & Business Media, 2012.
500   [10] X. Wang, Q. Xiao, C. Wu, P. Li, S. Xia, Fabrication of nanofiltration membrane on MoS2 modified
501   PVDF substrate for excellent permeability, salt rejection, and structural stability, Chem. Eng. J., 416
502   (2021) 129154.
503   [11] A.F. Alsayed, M.A. Ashraf, Modified nanofiltration membrane treatment of saline water, in:
504   Water Engineering Modeling and Mathematic Tools, Elsevier, 2021, pp. 25-44.
505   [12] Y. Yu, Y. Yang, L. Yu, K.Y. Koh, J.P. Chen, Modification of polyvinylidene fluoride membrane by
506   silver nanoparticles-graphene oxide hybrid nanosheet for effective membrane biofouling mitigation,
507   Chemosphere, 268 (2021) 129187.
508   [13] L. Zhu, M. Wu, B. Van der Bruggen, L. Lei, L. Zhu, Effect of TiO2 content on the properties of
509   polysulfone nanofiltration membranes modified with a layer of TiO2–graphene oxide, Sep. Purif.
510   Technol., (2020) 116770.
511   [14] Y. Xu, Y. Xiao, W. Zhang, H. Lin, L. Shen, R. Li, Y. Jiao, B.-Q. Liao, Plant polyphenol intermediated
512   metal-organic framework (MOF) membranes for efficient desalination, J. Membr. Sci., 618 (2021)
513   118726.
514   [15] J. Xue, J. Shen, R. Zhang, F. Wang, S. Liang, X. You, Q. Yu, Y. Hao, Y. Su, Z. Jiang, High-flux
515   nanofiltration membranes prepared with β-cyclodextrin and graphene quantum dots, J. Membr. Sci.,
516   612 (2020) 118465.
517   [16] S. Yadav, I. Ibrar, A. Altaee, A.K. Samal, R. Ghobadi, J. Zhou, Feasibility of brackish water and
518   landfill leachate treatment by GO/MoS2-PVA composite membranes, Sci. Total Environ., (2020)
519   141088.
520   [17] S. Yadav, I. Ibrar, A. Altaee, S. Déon, J. Zhou, Preparation of novel high permeability and antifouling
521   polysulfone-vanillin membrane, Desalination, 496 (2020) 114759.

522 [18] W. Liu, S. Hu, G. Liu, F. Pan, H. Wu, Z. Jiang, B. Wang, Z. Li, X. Cao, Creation of hierarchical
523 structures within membranes by incorporating mesoporous microcapsules for enhanced separation
524 performance and stability, Journal of Materials Chemistry A, 2 (2014) 5267-5279.
525 [19] M. Jyothi, S. Yadav, G. Balakrishna, Effective recovery of acids from egg waste incorporated PSf
526 membranes: A step towards sustainable development, J. Membr. Sci., 549 (2018) 227-235.
527 [20] D. Rana, T. Matsuura, Surface modifications for antifouling membranes, Chem. Rev., 110 (2010)
528 2448-2471.
529 [21] R.R. Choudhury, J.M. Gohil, S. Mohanty, S.K. Nayak, Antifouling, fouling release and antimicrobial
530 materials for surface modification of reverse osmosis and nanofiltration membranes, Journal of
531 Materials Chemistry A, 6 (2018) 313-333.
532 [22] X.-T. Yuan, L. Wu, H.-Z. Geng, L. Wang, W. Wang, X.-S. Yuan, B. He, Y.-X. Jiang, Y.-j. Ning, Z.-R. Zhu,
533 Polyaniline/polysulfone ultrafiltration membranes with improved permeability and anti-fouling
534 behavior, Journal of Water Process Engineering, 40 (2021) 101903.
535 [23] H. Nawaz, M. Umar, A. Ullah, H. Razzaq, K.M. Zia, X. Liu, Polyvinylidene fluoride nanocomposite
536 super hydrophilic membrane integrated with Polyaniline-Graphene oxide nano fillers for treatment of
537 textile effluents, J. Hazard. Mater., 403 (2021) 123587.
538 [24] L. Shu, L.-H. Xie, Y. Meng, T. Liu, C. Zhao, J.-R. Li, A thin and high loading two-dimensional MOF
539 nanosheet based mixed-matrix membrane for high permeance nanofiltration, J. Membr. Sci., 603
540 (2020) 118049.
541 [25] R.P. Pandey, P.A. Rasheed, T. Gomez, R.S. Azam, K.A. Mahmoud, A fouling-resistant mixed-matrix
542 nanofiltration membrane based on covalently cross-linked Ti_3C_2TX (MXene)/cellulose acetate, J.
543 Membr. Sci., 607 (2020) 118139.
544 [26] S. Homaeigohar, M. Elbahri, Graphene membranes for water desalination, NPG Asia Materials, 9
545 (2017) e427-e427.
546 [27] B. Ganesh, A.M. Isloor, A.F. Ismail, Enhanced hydrophilicity and salt rejection study of graphene
547 oxide-polysulfone mixed matrix membrane, Desalination, 313 (2013) 199-207.
548 [28] H. Wu, B. Tang, P. Wu, Development of novel SiO_2–GO nanohybrid/polysulfone membrane with
549 enhanced performance, J. Membr. Sci., 451 (2014) 94-102.
550 [29] E. Gomes, A. Rodrigues, Crystallization of vanillin from kraft lignin oxidation, Sep. Purif. Technol.,
551 (2020) 116977.
552 [30] N. Ahmad, A. Samavati, N.A.H.M. Nordin, J. Jaafar, A.F. Ismail, N.A.N.N. Malek, Enhanced
553 performance and antibacterial properties of amine-functionalized ZIF-8-decorated GO for
554 ultrafiltration membrane, Sep. Purif. Technol., 239 (2020) 116554.
555 [31] M. He, X. Fan, Z. Yang, R. Zhang, Y. Liu, L. Fan, Q. Zhang, Y. Su, Z. Jiang, Antifouling high-flux
556 membranes via surface segregation and phase separation controlled by the synergy of hydrophobic
557 and hydrogen bond interactions, J. Membr. Sci., 520 (2016) 814-822.
558 [32] P. Dutournié, S. Déon, L. Limousy, Understanding the separation of anion mixtures by TiO_2
559 membranes: Numerical investigation and effect of alkaline treatment on physicochemical properties,
560 Chem. Eng. J., 363 (2019) 365-373.
561 [33] S. Déon, A. Escoda, P. Fievet, P. Dutournié, P. Bourseau, How to use a multi-ionic transport model
562 to fully predict rejection of mineral salts by nanofiltration membranes, Chem. Eng. J., 189 (2012) 24-
563 31.
564 [34] S. Déon, A. Escoda, P. Fievet, R. Salut, Prediction of single salt rejection by NF membranes: An
565 experimental methodology to assess physical parameters from membrane and streaming potentials,
566 Desalination, 315 (2013) 37-45.
567 [35] M.D. Afonso, G. Hagmeyer, R. Gimbel, Streaming potential measurements to assess the variation
568 of nanofiltration membranes surface charge with the concentration of salt solutions, Sep. Purif.
569 Technol., 22 (2001) 529-541.
570 [36] A. Ghaffar, L. Zhang, X. Zhu, B. Chen, Scalable graphene oxide membranes with tunable water
571 channels and stability for ion rejection, Environmental Science: Nano, 6 (2019) 904-915.

572 [37] S. Saqib, S. Rafiq, N. Muhammad, A.L. Khan, A. Mukhtar, S. Ullah, M.H. Nawaz, F. Jamil, C. Zhang,
573 V. Ashokkumar, Sustainable mixed matrix membranes containing porphyrin and polysulfone polymer
574 for acid gas separations, J. Hazard. Mater., 411 (2021) 125155.
575 [38] D. Khalili, Graphene oxide: a promising carbocatalyst for the regioselective thiocyanation of
576 aromatic amines, phenols, anisols and enolizable ketones by hydrogen peroxide/KSCN in water, New
577 J. Chem., 40 (2016) 2547-2553.
578 [39] M. Zakertabrizi, E. Hosseini, A.H. Korayem, A. Razmjou, A.G. Fane, V. Chen, Insight from perfectly
579 selective and ultrafast proton transport through anhydrous asymmetrical graphene oxide membranes
580 under Grotthuss mechanism, J. Membr. Sci., 618 (2021) 118735.
581 [40] A. Alkhouzaam, H. Qiblawey, Novel polysulfone ultrafiltration membranes incorporating
582 polydopamine functionalized graphene oxide with enhanced flux and fouling resistance, J. Membr.
583 Sci., 620 (2021) 118900.
584 [41] K. Sunil, G. Karunakaran, S. Yadav, M. Padaki, V. Zadorozhnyy, R.K. Pai, Al-Ti2O6 a mixed metal
585 oxide based composite membrane: A unique membrane for removal of heavy metals, Chem. Eng. J.,
586 348 (2018) 678-684.
587 [42] K. Dutta, S. Das, P.P. Kundu, Low methanol permeable and highly selective membranes composed
588 of pure and/or partially sulfonated PVdF-co-HFP and polyaniline, J. Membr. Sci., 468 (2014) 42-51.
589 [43] C. Klaysom, R. Marschall, S.-H. Moon, B.P. Ladewig, G.M. Lu, L. Wang, Preparation of porous
590 composite ion-exchange membranes for desalination application, J. Mater. Chem., 21 (2011) 7401-
591 7409.
592 [44] R. Kingsbury, K. Bruning, S. Zhu, S. Flotron, C. Miller, O. Coronell, Influence of water uptake,
593 charge, manning parameter, and contact angle on water and salt transport in commercial ion
594 exchange membranes, Ind. Eng. Chem. Res., 58 (2019) 18663-18674.
595 [45] N. Agmon, The grotthuss mechanism, Chem. Phys. Lett., 244 (1995) 456-462.
596 [46] A. Hassanali, F. Giberti, J. Cuny, T.D. Kühne, M. Parrinello, Proton transfer through the water
597 gossamer, Proceedings of the National Academy of Sciences, 110 (2013) 13723-13728.
598 [47] Y. Manawi, V. Kochkodan, A. Mohammad, M.A. Atieh, Arabic gum as a novel pore-forming and
599 hydrophilic agent in polysulfone membranes, J. Membr. Sci., 529 (2017) 95-104.
600 [48] D. Breite, M. Went, A. Prager, A. Schulze, The critical zeta potential of polymer membranes: how
601 electrolytes impact membrane fouling, RSC advances, 6 (2016) 98180-98189.
602 [49] L.-S. Wan, Z.-K. Xu, X.-J. Huang, Approaches to Protein Resistance on The Polyacrylonitrile-Based
603 Membrane Surface: An Overview, Proteins at Solid-Liquid Interfaces, (2006) 245-269.
604 [50] A.F. Ibrahim, Y. Lin, Synthesis of graphene oxide membranes on polyester substrate by spray
605 coating for gas separation, Chem. Eng. Sci., 190 (2018) 312-319.
606 [51] I. Alam, L.M. Guiney, M.C. Hersam, I. Chowdhury, Antifouling properties of two-dimensional
607 molybdenum disulfide and graphene oxide, Environmental Science: Nano, 5 (2018) 1628-1639.
608 [52] S.T. Kelly, A.L. Zydney, Effects of intermolecular thiol–disulfide interchange reactions on bsa
609 fouling during microfiltration, Biotechnology and bioengineering, 44 (1994) 972-982.

610